Title
Northwestern Pacific typhoon intensity controlled by changes in ocean temperatures.

Journal
Science advances, 1(4)

ISSN
2375-2548

Authors
Mei, Wei
Xie, Shang-Ping
Primeau, François
et al.

Publication Date
2015-05-01

DOI
10.1126/sciadv.1500014

ATMOSPHERIC SCIENCE

10.1126/sciadv.1500014

Northwestern Pacific typhoon intensity controlled by changes in ocean temperatures

Wei Mei,[1,2]* Shang-Ping Xie,[1] François Primeau,[2] James C. McWilliams,[3] Claudia Pasquero[4]

Dominant climatic factors controlling the lifetime peak intensity of typhoons are determined from six decades of Pacific typhoon data. We find that upper ocean temperatures in the low-latitude northwestern Pacific (LLNWP) and sea surface temperatures in the central equatorial Pacific control the seasonal average lifetime peak intensity by setting the rate and duration of typhoon intensification, respectively. An anomalously strong LLNWP upper ocean warming has favored increased intensification rates and led to unprecedentedly high average typhoon intensity during the recent global warming hiatus period, despite a reduction in intensification duration tied to the central equatorial Pacific surface cooling. Continued LLNWP upper ocean warming as predicted under a moderate [that is, Representative Concentration Pathway (RCP) 4.5] climate change scenario is expected to further increase the average typhoon intensity by an additional 14% by 2100.

INTRODUCTION

Tropical cyclones (TCs) are among the most devastating and destructive natural hazards on Earth (*1*, *2*), with the most intense TCs found over the northwestern Pacific. Super Typhoon Haiyan of 2013, one of the strongest TCs in history over the northwestern Pacific, caused more than 6200 deaths with additional 1785 people reported missing in the Philippines alone (*3*). In theory, a potential intensity (PI) exists and can be predicted with a given sea surface temperature (SST) and atmospheric thermodynamic profile (*4*, *5*). Unfortunately, the intensity of individual TCs is extremely difficult to predict in reality (*6*) because of various internal and environmental factors involved in the evolution of TC intensity (*7*, *8*), such as vertical shear of horizontal winds in the troposphere (*9*) and interaction of the TC with the ocean (*8*, *10*–*14*). The challenge extends to and becomes even bigger for prediction and projection of TC intensity on time scales beyond a season (*15*). Adding to the challenge is the fact that the climate models in use do not have sufficient spatial resolution to adequately resolve TC structure and intensity, although some of them are skillful in reproducing year-to-year changes in seasonal TC counts and track density (*16*–*18*). The projected changes in TC intensity under global warming vary widely among models with large and poorly quantified uncertainties (*19*). Alternatively, a statistical approach that links the seasonal mean TC intensity to climate indices can be very helpful both for the projections and as a guide to understanding the relevant factors that govern mean TC activity. Here, we disentangle the causes of the interannual-to-decadal variability of the lifetime peak TC intensity in the northwestern Pacific where TCs are most active. We restrict our attention to TCs that reach at least typhoon intensity (equivalent to category 1 hurricane intensity in the North Atlantic). We focus on the year-to-year variability of the seasonal mean lifetime peak intensity (obtained from the lifetime peak intensity of all TCs over the entire typhoon season for each year; see Materials and Methods) instead of the variability among individual TCs because the dominant factors for the latter vary from case to case.

[1]Scripps Institution of Oceanography, University of California, San Diego, San Diego, CA 92093, USA. [2]Department of Earth System Science, University of California, Irvine, Irvine, CA 92697, USA. [3]Department of Atmospheric and Oceanic Sciences, University of California, Los Angeles, Los Angeles, CA 90095, USA. [4]Department of Earth and Environmental Sciences, University of Milano-Bicocca, I-20126 Milan, Italy.
*Corresponding author. E-mail: wmei@ucsd.edu

RESULTS

Figure 1A shows the evolution of the seasonal mean lifetime peak intensity of typhoons between 1951 and 2010, computed using TC data from the Joint Typhoon Warning Center (JTWC) best track data set (*20*), with the intensity data before 1973 being adjusted to account for shifting wind-pressure relationships. Significant interannual-to-decadal variability is evident with a period of weak decrease from the late 1950s to the mid-1970s followed by a rising trend. The mean lifetime peak intensity during the last two decades is about 5 m s^{-1} (~10%) higher than that in the 1970s, corresponding to a 33% increase in the instantaneous destructiveness of typhoons that scales as the cube of wind speed (*21*). Similar results for the seasonal mean lifetime peak intensity and other typhoon metrics to be discussed later (for example, intensification rate and duration) are obtained using the maximum 1-min sustained wind speed converted from the Japan Meteorological Agency best track data (fig. S1; see the Supplementary Materials for details). Analysis of the distribution of typhoon lifetime peak intensity within individual years shows that the increase in seasonal mean peak values is due to an increase in the proportion of stronger typhoons (fig. S2), consistent with previous findings (*21*–*26*).

The lifetime peak intensity achieved by a TC can be written as

$$v_{max} = v_0 + I \times D \quad (1)$$

where v_0 is the intensity of the TC when it reaches typhoon intensity for the first time and can be considered as a constant (~33 m s^{-1}), I is the mean intensification rate from v_0 to v_{max}, and D is the corresponding intensification duration. Accordingly, to gain new insights into the physical mechanisms underlying the variability in the seasonal mean lifetime peak intensity, we take a new approach and view v_{max} as a product of two factors: the rate of intensification (I) and the duration of intensification (D). The seasonal mean values of intensification rate and intensification duration exhibit strong variations (Fig. 1, B and C) and are not correlated (cross-correlation $r = -0.07$), and their product well represents the variations in seasonal mean lifetime peak intensity (Fig. 1A; the correlation coefficient between the solid and dashed curves is ~0.9). In particular, despite a reduction in the duration of typhoon intensification during the recent decade, the lifetime peak intensity remains unchanged because of an unprecedentedly high intensification

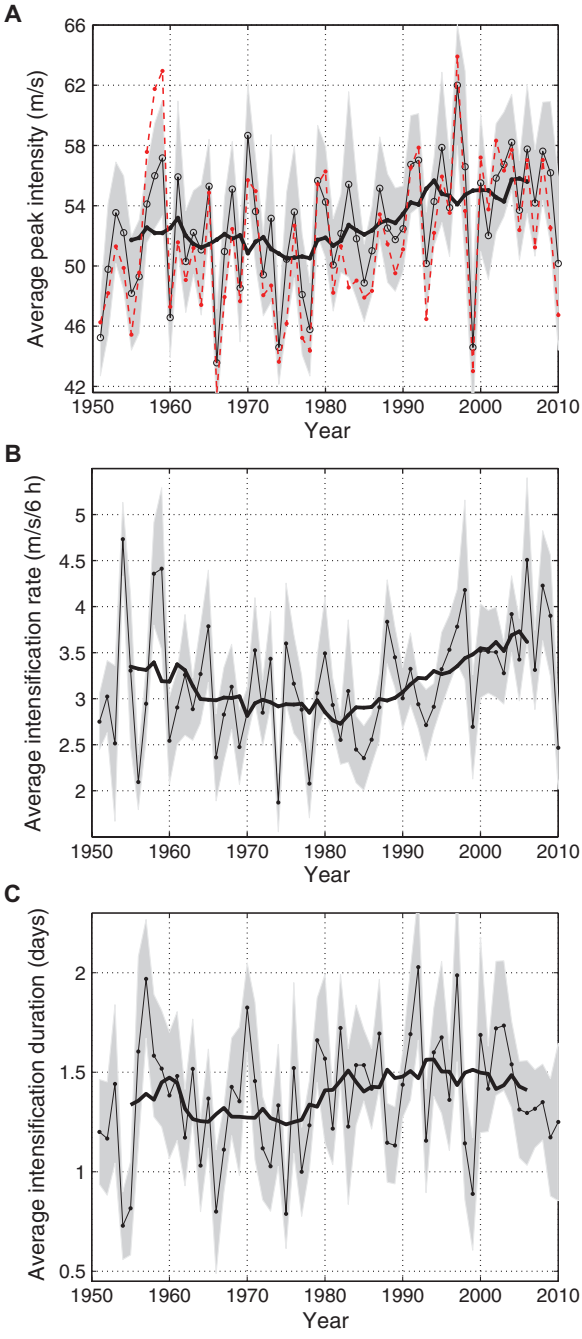

Fig. 1. Interannual-to-decadal variability of various typhoon metrics. (**A** to **C**) Seasonal mean (A) lifetime peak intensity ($\overline{v_{max}}$), (B) intensification rate ($\bar{I}$), and (C) intensification duration ($\bar{D}$) of typhoons in the northwestern Pacific as a function of time (thin solid black curve). The thick black curve in each panel shows the 9-year running averages. Error bars shown as shading are calculated by dividing the SD by the square root of the number of storms in each year. The thin dashed red curve in (A) is obtained as $v_0 + \bar{I} \times \bar{D}$, and its correlation with $\overline{v_{max}}$ (thin solid black curve) is 0.89.

rate. The nonsignificant relationship between the seasonal mean intensification rate and duration suggests that they are influenced by different factors.

Factors that have been identified as being potentially important for setting the intensification rate are the SST, upper ocean thermal state, vertical wind shear, low-level vorticity, and the thermodynamic state of the atmosphere (*8*–*10*, *12*, *27*–*33*). We computed the correlation coefficient between the seasonal mean intensification rate and the vertical shear of horizontal winds, of zonal and meridional components, low-level vorticity, mid-level vertical velocity, sea-level pressure, PI, SST, SST relative to global or Pacific tropical mean value, and subsurface water temperatures, all averaged over the main intensification region [fig. S3; and this region is referred to as the low-latitude northwestern Pacific (LLNWP) in the abstract], and also the PI averaged over the genesis region defined in ref. (*21*) (5°N to 15°N, 130°E to 180°E). We find that ocean temperatures in the typhoon intensification region dominate over the other factors in explaining the variability in the seasonal mean typhoon intensification rate (Fig. 2A and Table 1). The highest correlation is found in the subsurface (~50 to 150 m) (Fig. 2A). The seasonal mean intensification rate is not significantly correlated with atmospheric variables except for PI, which is closely related to the SST, although preliminary analysis suggests that atmospheric conditions may be more important for variations among individual TCs within a given season or for the seasonal mean intensification rates at the pretyphoon stage. In addition, changes in SST over the typhoon intensification region relative to global or Pacific tropical mean SST do not seem to play an important role in affecting intensification rate, although the relative SST changes are important for other TC metrics (such as counts) (*19*, *31*, *34*, *35*).

Correlation does not imply causality, but the ocean effect on TCs has a sound physical basis. SST affects PI (*36*, *37*), and subsurface thermal stratification influences the amplitude of typhoon-induced SST cooling (*38*). To quantify their respective importance in the seasonal mean intensification rate ($\bar{I}$), we use a regression model:

$$\bar{I} = a\mathrm{SST} + bT_{\mathrm{sub}} + c \quad (2)$$

with T_{sub} representing subsurface ocean temperature and c being a constant (*39*). This model can be further written as follows:

$$\bar{I} = (a+b)\mathrm{SST} - b(\mathrm{SST} - T_{\mathrm{sub}}) + c \quad (3)$$

to delineate the respective effect of SST and subsurface stratification (SST − T_{sub}) (*40*). Assigning T_{sub} and SST, respectively, with anomalies in 75-m ocean temperature and SST with respect to their respective long-term climatological mean, we obtain a = 0.08 m s^{-1} per 6 hours per °C, b = 1.03 m s^{-1} per 6 hours per °C, and c = 3.10 m s^{-1} per 6 hours. This suggests that (i) a warmer SST and/or a weaker stratification favor typhoon intensification; (ii) changes in SST and subsurface stratification are nearly equally important in influencing seasonal mean intensification rate (because their semipartial correlations with intensification rate are nearly equal in magnitude at 0.48 and −0.51, respectively); and (iii) intensification rate variations can be viewed as being largely due to subsurface temperature changes that include information on changes in both SST and subsurface stratification ($\Delta\bar{I} \sim \Delta T_{\mathrm{sub}}$). The robustness of the correlation between $\bar{I}$ and T_{sub} (r = 0.58; Fig. 2, A and B, and Table 1) is confirmed by a Bayesian uncertainty analysis (see Materials and Methods) that explicitly takes into account the autocorrelation in water temperature. During the past three decades, a 0.75°C rise in 75-m water temperature coincides with an increase of nearly 0.8 m s^{-1} per 6 hours in the mean intensification rate (from 2.8 to 3.6 m s^{-1} per 6 hours). Consistent with this, our

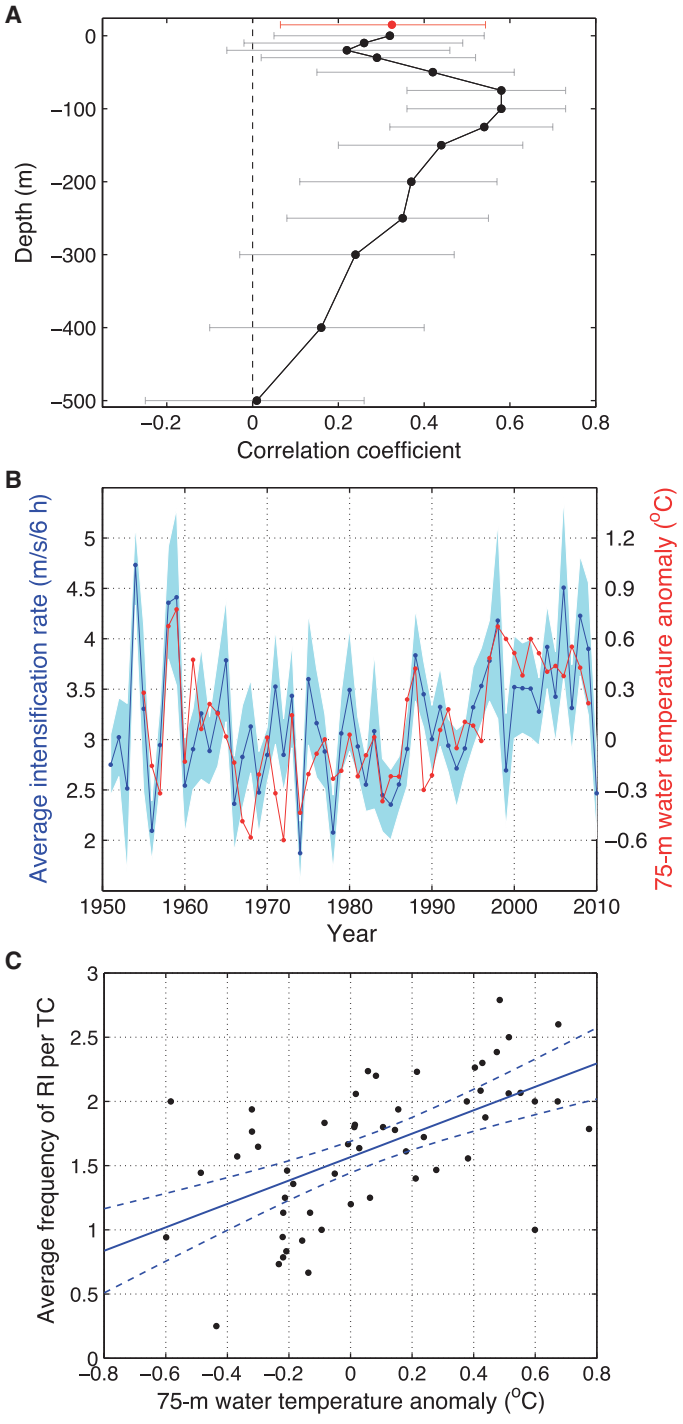

Fig. 2. Typhoon intensification rate versus ocean temperatures. (**A**) Correlation between seasonal mean intensification rate and summer (July–September) ocean temperatures at different depths (black dots) and PI (red dot) averaged over the intensification region. Gray and red bars show the 95% credible intervals. (**B**) Time series of seasonal mean intensification rate (blue curve) and ocean temperature at 75-m depth averaged over the intensification region (red curve). (**C**) Scatter plot of seasonal mean frequency of rapid intensification per storm versus ocean temperature at 75-m depth averaged over the intensification region. Solid blue line shows the linear regression, with dashed blue curves showing the 95% confidence bands.

Table 1. Correlation between typhoon intensification rate and various atmospheric and oceanic variables. $|\Delta V|_{200-850}$, full shear; $|\Delta u|_{200-850}$, shear of zonal wind; $|\Delta v|_{200-850}$, shear of meridional wind; ζ_{850}, 850-hPa vorticity; ω_{500}, 500-hPa pressure velocity; SLP, sea-level pressure; PI_{inten}, PI over the main intensification region; $PI_{genesis}$, PI over the main genesis region defined in ref. (*21*); RSST, SST over the typhoon intensification region relative to global tropical mean SST; T_{75m}, ocean temperature at 75-m depth; r_{upper} and r_{lower}, the upper and lower bounds, respectively, for a 95% credible interval.

	$\|\Delta V\|$	$\|\Delta u\|$	$\|\Delta v\|$	ζ_{850}	ω_{500}	SLP	PI_{inten}	$PI_{genesis}$	SST	RSST	T_{75m}
r	−0.17	0.13	−0.03	−0.18	0.07	0.16	0.33	−0.03	0.32	0.09	0.58
r_{upper}	0.10	0.38	0.24	0.09	0.33	0.41	0.54	0.23	0.54	0.35	0.36
r_{lower}	−0.42	−0.14	−0.29	−0.43	−0.20	−0.11	0.07	−0.30	0.05	−0.18	0.73

observational analysis shows that warmer subsurface waters favor rapid intensification (defined as intensification rate ≥4.5 m s^{-1} per 6 hours; Fig. 2C).

The effectiveness of subsurface water temperatures in affecting typhoon development depends on how quickly the subsurface water can be brought to the surface. We have simulated the oceanic response to the passage of a typhoon using an ocean circulation model (see Materials and Methods). By adding passive tracers at different depths, we show that water at 75-m depth can be brought to the surface 6 hours before the passage of the typhoon eye as a result of wind-induced upwelling and vertical mixing (fig. S6; about 50% of the water in the 30-m-deep, pre-typhoon mixed layer has been replaced by water originating from depths between 50 and 100 m), consistent with observational analysis of SST (*41*). Water at 125-m depth appears at the surface at a later time, but it still modulates the amplitude of the SST cooling before the passage of the second half of typhoon eyewall (fig. S6). Because TC-generated SST cooling can induce a nearly instantaneous response in TC intensity (*42*), subsurface temperatures exert a strong effect on typhoon development.

We have further compared our estimates with previous theoretical, observational, and modeling results by considering two situations. On the one hand, for a fixed subsurface stratification, Eq. 3 suggests that a 1°C increase in background SST (with an accompanied 1°C increase in T_{sub}) would increase the intensification rate by ~1 m s^{-1} per 6 hours and thereby the intensity by ~5 m s^{-1}. This sensitivity of typhoon intensity to SST is consistent with previous theoretical and modeling studies [that is, 1 to 10 m s^{-1} per °C; for example, see refs. (*36*, *43*–*45*) for PI considerations; see refs. (*46*–*48*) for simulations using the GFDL Hurricane Prediction System or Weather and Research Forecasting model]. On the other hand, for a fixed background SST, Eq. 2 or Eq. 3 suggests that a 1°C reduction in T_{sub} (that is, a 1°C increase in the subsurface stratification SST − T_{sub}) would reduce the intensification rate by ~1 m s^{-1} per 6 hours because of the cooler instantaneous SST experienced by the typhoon. For a typical mixed layer depth of 30 m (fig. S4A), the induced SST cooling would be ~0.7°C, assuming that during its passage the typhoon can sufficiently mix the top 100 m of the water column to produce a uniform temperature profile (*49*). This indicates that the sensitivity of the intensification rate to the negative SST feedback associated with the typhoon-induced instantaneous cooling is ~(1 m s^{-1} per 6 hours)/(0.7°C) ≈ 1.4 m s^{-1} per 6 hours per °C. This is in accord with the observational results shown in ref. (*13*) and modeling results shown in ref. (*32*).

The duration of typhoon intensification, on the other hand, is, by definition, related to the length of the path and the translation speed. Here, we represent the length of the path simply using the difference between the seasonal mean starting ($*_{str}$) and ending ($*_{end}$) longitude (ϕ) and latitude (λ) of the intensification stage. Correlation calculations show that the path length dominates over the translation speed (U) for the variations of intensification duration (table S1).

Furthermore, this path length is largely determined by the longitude and latitude of typhoon genesis. This is not surprising: When a typhoon forms closer to the equator and the dateline, it can intensify for a longer period of time over warm water, before reaching land or cold water. This is confirmed by the high correlation between the seasonal mean intensification duration and El Niño Southern Oscillation (ENSO) and the Pacific Decadal Oscillation (PDO) indices (Fig. 3 and table S1). In a positive phase of ENSO/PDO, warm water extends eastward over the tropical Pacific, producing a large-scale atmospheric environment over the southeastern quadrant of the northwestern Pacific (for example, above-normal low-level vorticity and mid-level upward motion) that favors a southeastward displacement of TC/typhoon genesis (*18*, *29*, *50*–*52*). As a result, the average duration of typhoon intensification is longer during the 1990s compared to the mid-1970s (Fig. 1C). The duration shortens during the last decade (Fig. 1C) owing to the cooling of the central equatorial Pacific (Fig. 3) (*53*), contributing negatively to the seasonal mean lifetime peak intensity. This effect is, however, compensated and even surpassed in size by that of enhanced intensification rate due to upper ocean warming in the typhoon intensification region (that is, LLNWP), making typhoon intensity of the last decade on average the strongest over the past six decades (Fig. 1A).

Because measurements of TC intensity have evolved with time over the northwestern Pacific, we have further performed the following sensitivity analyses to test the robustness of our results (see the Supplementary Materials for details). First, we repeated the calculations with more reliable data for recent decades. We found that the relationship between intensification rate and ocean temperatures and that between intensification duration and ENSO/PDO remain generally unchanged. Second, to remove the effect of slow changes in observational methods, we repeated the analysis for 9-year high-pass filtered data and obtained similar results. Furthermore, the intensity data from different agencies are generally consistent, as discussed earlier. All of these examinations suggest that our results are robust.

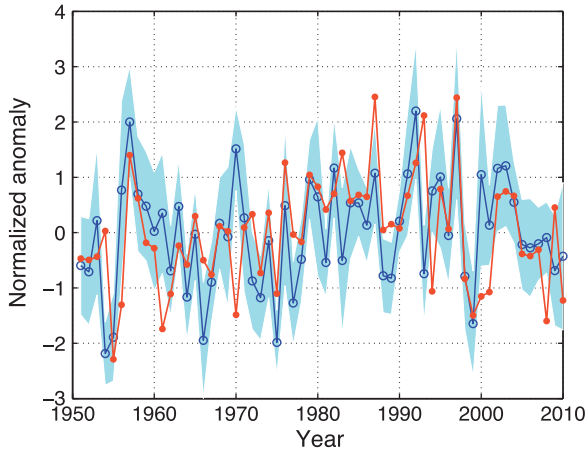

Fig. 3. Modulation of typhoon intensification duration by PDO. Time series of normalized seasonal mean duration of typhoon intensification (blue curve) and normalized PDO index during the typhoon peak season (red curve). The correlation coefficient between them is 0.43.

DISCUSSION

Our observational analysis has thus revealed that the seasonal mean typhoon lifetime peak intensity is primarily controlled by two distinct factors: intensification rate, which in turn is strongly affected by local upper ocean temperatures, and intensification duration, which in turn is influenced by large-scale modes of climate variability. The findings, to our knowledge, provide the first observational evidence for the dominance of upper ocean thermal structure in the interannual-to-decadal variability of typhoon lifetime peak intensity and are in line with the predictions obtained in recent modeling work of ref. (*32*), and hence emphasize the importance of monitoring ocean subsurface temperatures for the prediction of TC intensity (*14*, *54*–*58*).

Our results have important implications for changes in typhoon lifetime peak intensity under global warming. In response to strengthened greenhouse gas forcing, the SST increase acts to intensify typhoons, whereas intensified upper ocean stratification suppresses typhoon intensification. Previous projections of typhoon intensity measured by maximum wind speed or minimum central pressure based on PI theory and dynamical models vary widely between −2 and 17.3% (*19*). These projections, however, may have large uncertainties, because the original PI theory does not include the ocean coupling processes and dynamical models do not have sufficient spatial resolution to simulate observed intensity. Here, we provide the first statistical projection using our observation-based regression model that considers both the effects of SST and subsurface stratification. In 20 models (table S2) from the fifth phase of the Coupled Model Intercomparison Project (CMIP5) (*59*), ocean surface and subsurface temperatures in the typhoon intensification region (that is, LLNWP) warm by 1.4° and 1.3°C, respectively, by the end of this century under Representative Concentration Pathway (RCP) 4.5 (a medium mitigation scenario) (fig. S7). Applying our regression model to CMIP5 projections and assuming both PDO and ENSO in their neutral states, we find that the seasonal mean typhoon lifetime peak intensity may increase from the current 55 m s^{-1} (category 3) to 62.5 m s^{-1} (category 4) (Fig. 4). This projected increase in typhoon intensity is largely due to SST warming because changes in subsurface stratification are small, in contrast to natural variability where the thermal stratification variability is as important as SST (Eq. 3 and Fig. 2). Our statistical model's projected percentage increase (14%) in typhoon intensity is at the high end of previous PI and dynamical model projections (*19*). A caveat is that our statistical model may omit some physical processes that are insignificant in current climate variability but may become important for typhoon intensification under global warming, such as the lapse rate effect (*60*, *61*) (see the Supplementary Materials for a detailed discussion). Those processes may bring uncertainty to the size of our projected intensity increase—an interesting topic we leave for a future study—but we believe that their inclusion should not change our main conclusion. The strengthened typhoon intensity poses heightened threats to human society and marine/terrestrial ecosystems (*1*, *2*, *62*, *63*). Meanwhile, the intensification of these powerful storms may accelerate ocean warming and affect heat transport in both the ocean and the atmosphere (*49*, *64*–*68*).

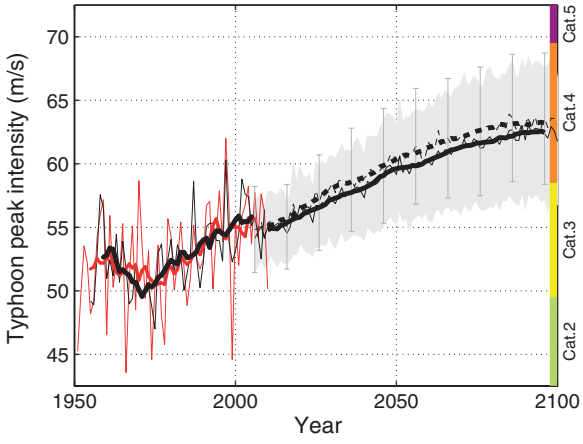

Fig. 4. Observed and projected typhoon lifetime peak intensity. Observed (thin red), predicted (1950–2009; thin black), and projected (2006–2100; thin black) seasonal mean typhoon lifetime peak intensity (m s^{-1}) and their 9-year running means (thick curves). Two projections are given: one (solid) considers both changes in SST and subsurface stratification with continuous gray shading showing error bars, and the other (dashed) ignores changes in subsurface stratification with error bars shown discretely for years 2006, 2016, …, and 2096. See Materials and Methods for details. The colors on the right *y* axis denote the range of typhoon intensity from category 2 up to category 5 based on the Saffir-Simpson hurricane scale.

MATERIALS AND METHODS

Observational data

The TC data over the northwestern Pacific are from the JTWC best track data set (*20*), which provides TC location and intensity at 6-hour intervals. A time period of 60 years of the data (1951–2010) is in use, which allows an examination of variations over long time scales such as the decadal time scale. Note that there have been adjustments to intensity data before 1973, designed to account for shifting wind-pressure relationships used by JTWC (see details in ftp://texmex.mit.edu/pub/emanuel/HURR/tracks_netcdf/readme_netcdf.pdf). We focus on TCs that reach typhoon intensity (~33 m s^{-1}) because of their marked influences in many aspects and strong coupling with the ocean. To focus on the effect of atmospheric and oceanic conditions, we excluded a small fraction of typhoons that are influenced by land in the calculation, although including them produces very similar results. In total, there are more than 850 typhoons used in this study. Note that in this study, we do not consider variations in TC/typhoon counts because they are determined by other factors. As shown in refs. (*18*, *51*), the number of TCs/typhoons in a given year is related to the frequency of TC genesis, which in turn is largely determined by SSTs over the northern off-equatorial central Pacific.

For each typhoon location, the intensification rate is computed by central differencing the maximum 1-min sustained surface wind speed at a 12-hour interval. A rapid intensification event is identified when the intensification rate is ≥4.5 m s^{-1} per 6 hours; using a different criterion (for example, 4 or 5 m s^{-1} per 6 hours) does not change the conclusion shown in Fig. 2C. Translation speed is calculated by dividing the sum of the respective distance the typhoon moves 6 hours before and 6 hours after reaching the current position by the total time interval (that is, 12 hours), using the positions reported in the best track data. Then, for each individual typhoon, we can get a mean value of intensification rate and mean translation speed by simply averaging the values at all locations during its intensification period (that is, from the TC reaching typhoon intensity for the first time until its lifetime peak intensity), and the duration of intensification is accordingly defined as the length of this intensification period. Because here we are more interested in the variation in the seasonal mean, the mean intensification rate, mean translation speed, and duration of intensification of each typhoon are then used to calculate the seasonal mean values using all typhoons during that season.

Atmospheric variables including zonal and meridional winds, air temperature, pressure, and relative humidity from National Centers for Environmental Prediction (NCEP)/National Center for Atmospheric Research (NCAR) Reanalysis 1 (*69*), SSTs from the Hadley Centre SST data set (*70*), the PDO index from http://jisao.washington.edu/pdo/PDO.latest, and ocean temperature anomalies from the World Ocean Database 2009 (*71*) are used to identify the mechanisms underlying the variability in seasonal mean typhoon intensification rate and intensification duration. The first three data sets have a monthly temporal resolution, and the last one has a temporal resolution of 3 months (that is, January–March, April–June, July–September, and October–December for each year) and is available since 1955. Because the northwestern Pacific typhoons are most active in the summer season [see, for example, ref. (*72*)] and the ocean temperature data have a 3-month resolution, here we use the data during July–September to represent the typical atmospheric and oceanic conditions during the typhoon season. We tested the sensitivity of the results using data between July and October for variables with a monthly resolution, and reached the same conclusions. The typhoon intensification region used to calculate the mean value of various atmospheric and oceanic variables is defined on the basis of the geographic distribution of the locations where typhoons experience intensification during the study period (fig. S3).

We regress the seasonal mean intensification rate onto observed SST and 75-m ocean temperature anomalies, and obtain $\bar{I}_{sim} = 0.08 \times SST + 1.03 \times T_{sub} + 3.10$ (that is, Eq. 2 in the main text). Similarly, we regress the seasonal mean intensification duration onto observed Niño4 and PDO indices, and obtain $\overline{D}_{sim} = 0.08 \times PDO + 0.17 \times Niño4 + 1.39$. Using these two regression models, we obtain $\overline{v_{max}}_{sim} = v_0 + \bar{I}_{sim} \times \overline{D}_{sim}$ and show it as the predicted values in Fig. 4. We further project changes in the seasonal mean typhoon lifetime peak intensity, using these two empirical relations and projected ocean temperature anomalies in fig. S7, and assuming that both ENSO and PDO are in their neutral states. The results are shown as the thin solid black curve between 2006 and 2100 in Fig. 4. The error bars are calculated using uncertainties in the regression coefficients and spreading of projected ocean temperatures as well as SDs in both Niño4 and PDO indices, and are shown as continuous gray shading in Fig. 4. To compare the relative importance of changes in SST and subsurface thermal stratification in projected changes in typhoon lifetime peak intensity, we repeat the projection with $\bar{I}_{sim}$ calculated using Eq. 3 with the second term [that is, $b(SST - T_{sub})$] omitted to ignore the effect of changes in subsurface stratification, and show the results as the thin dashed black curve in Fig. 4. The corresponding error bars are calculated in the same way as for the gray shading and are shown discretely only for years 2006, 2016, …, 2086, and 2096.

Estimation of the correlation coefficient

We estimate the correlation coefficient between variables *X* and *Y* using a Bayesian approach. Assume that *X* and *Y* are correlated time

series with correlation coefficient ρ and variances σ_X^2 and σ_Y^2, respectively. The covariance matrix can be written as

$$C = \begin{pmatrix} \sigma_X^2 & \rho\sigma_X\sigma_Y \\ \rho\sigma_X\sigma_Y & \sigma_Y^2 \end{pmatrix}.$$

We can relate X and Y to uncorrelated white noise $\epsilon_1 \sim N(0, 1)$ and $\epsilon_2 \sim N(0, 1)$ using

$$\begin{pmatrix} X \\ Y \end{pmatrix} = \begin{pmatrix} \sigma_X & 0 \\ \rho\sigma_Y & \sigma_Y\sqrt{(1-\rho^2)} \end{pmatrix} \begin{pmatrix} \epsilon_1 \\ \epsilon_2 \end{pmatrix},$$

where the 2 by 2 matrix is the Cholesky decomposition of C. Inverting this equation gives

$$\begin{aligned} \begin{bmatrix} \epsilon_1 \\ \epsilon_2 \end{bmatrix} &= \begin{bmatrix} \sigma_X & 0 \\ \rho\sigma_Y & \sigma_Y\sqrt{(1-\rho^2)} \end{bmatrix}^{-1} \begin{bmatrix} X \\ Y \end{bmatrix} \\ &= \frac{1}{\sigma_X\sigma_Y\sqrt{(1-\rho^2)}} \begin{bmatrix} \sigma_Y\sqrt{(1-\rho^2)} & 0 \\ -\rho\sigma_Y & \sigma_X \end{bmatrix} \begin{bmatrix} X \\ Y \end{bmatrix}, \end{aligned}$$

which allows us to compute the Jacobian

$$J = \begin{bmatrix} \frac{\partial\epsilon_1}{\partial X} & \frac{\partial\epsilon_1}{\partial Y} \\ \frac{\partial\epsilon_2}{\partial X} & \frac{\partial\epsilon_2}{\partial Y} \end{bmatrix} = \begin{bmatrix} \frac{1}{\sigma_X} & 0 \\ -\frac{\rho}{\sigma_X\sqrt{1-\rho^2}} & \frac{1}{\sigma_Y\sqrt{1-\rho^2}} \end{bmatrix}$$

for the change of variables between the uncorrelated variables and the correlated variables. The joint density for X and Y can therefore be expressed as follows:

$$\begin{aligned} f(X,Y) &= f(\epsilon_1,\epsilon_2)|J| \\ &= \frac{1}{2\pi}\exp\left[-\frac{1}{2}\left(\epsilon_1^2+\epsilon_2^2\right)\right]|J| \\ &= \frac{1}{2\pi\sigma_X\sigma_Y\sqrt{1-\rho^2}}\exp\left[-\frac{1}{2(1-\rho^2)}\left(\frac{X^2}{\sigma_X^2}-\frac{2\rho XY}{\sigma_X\sigma_Y}+\frac{Y^2}{\sigma_Y^2}\right)\right] \\ &= \frac{1}{2\pi\sqrt{|C|}}\exp\left[-\frac{1}{2}(X,Y)C^{-1}\begin{pmatrix} X \\ Y \end{pmatrix}\right]. \end{aligned}$$

so that the likelihood function (that is, the probability of X and Y given σ_X, σ_Y, and ρ) is given by

$$\Pr((X,Y)|\sigma_X,\sigma_Y,\rho) = \frac{1}{(2\pi)^{N/2}(\det C)^{1/2}}\exp\left[-\frac{1}{2}(X,Y)C^{-1}\begin{pmatrix} X \\ Y \end{pmatrix}\right]$$

$$= \frac{1}{(2\pi)^{N/2}\sigma_X^N\sigma_Y^N(1-\rho^2)^{N/2}}\exp\left[-\frac{1}{2(1-\rho^2)}\sum_{i=1}^{N}\left(\frac{X_i^2}{\sigma_X^2}+\frac{Y_i^2}{\sigma_Y^2}-2\rho\frac{X_i}{\sigma_X}\frac{Y_i}{\sigma_Y}\right)\right].$$

Assigning a flat prior, the posterior probability is simply proportional to the likelihood.

In some of our calculations, X represents ocean temperatures and Y represents a metric of typhoons (such as intensification rate). Then, we need to consider the autocorrelation in the ocean temperature X. Denoting the autocorrelation of X by α, the posterior probability for σ_X, σ_Y, ρ, α becomes

$$\Pr(\sigma_X,\sigma_Y,\rho,\alpha|(X,Y)) \propto$$

$$\frac{\exp\left\{-\frac{1}{2(1-\rho^2)}\sum_{i=1}^{N-1}\left[\frac{(X_{i+1}-\alpha X_i)^2}{\sigma_X^2}+\frac{Y_{i+1}^2}{\sigma_Y^2}-2\rho\frac{(X_{i+1}-\alpha X_i)}{\sigma_X}\frac{Y_{i+1}}{\sigma_Y}\right]\right\}}{(2\pi)^{(N-1)/2}\sigma_X^{N-1}\sigma_Y^{N-1}(1-\rho^2)^{(N-1)/2}}$$

where we have assumed a flat prior for $\Pr(\sigma_X, \sigma_Y, \rho, \alpha)$.

Then, $\Pr(\rho|(X, Y))$ can be obtained as

$$\Pr(\rho|(X,Y)) = \int_0^{+\infty}\int_0^{+\infty}\int_{-\infty}^{+\infty}\Pr(\sigma_X,\sigma_Y,\rho,\alpha|(X,Y))\,d\alpha\,d\sigma_X\,d\sigma_Y.$$

From the posterior distribution of ρ [that is, $\Pr(\rho|(X, Y))$], we can get the most likely value of ρ and a corresponding 95% credible interval (Bayesian analog of a 95% confidence interval).

A numerical simulation of ocean temperature response to a typhoon

We use a primitive equation ocean model, the Regional Ocean Modeling System (ROMS) (*73*), to simulate the three-dimensional ocean response to a typhoon, with an aim to test whether the temperature anomalies at depths can feed back onto the typhoon development during the typhoon passage. The description of the simulation presented below largely parallels that of ref. (*74*).

We run ROMS in an idealized channel configuration on a β plane, subject to wind stress forcing associated with a typhoon. The domain is centered at 20°N in the meridional direction with $f = 5.0 \times 10^{-5}$ s^{-1} and $\beta = 2.14 \times 10^{-11}$ s^{-1} m^{-1}, and has a size of 4960 km × 6640 km × 5000 m ($L_x \times L_y \times H$) using periodic east-west lateral boundary conditions, and wall boundaries at the northern and southern edges. The horizontal resolution is 10 km, and in the vertical, there are 100 unequally spaced σ layers with 20 layers in the upper 100 m. The simulation is 10 days long, using a time step of 300 s. Third-order upstream bias horizontal advection is used for both temperature and momentum, and fourth-order centered vertical advection is used for temperature. Harmonic horizontal mixing is used for both temperature and momentum. The nonlocal *K*-profile parameterization scheme (*75*) is chosen to parameterize the vertical turbulent mixing.

The model ocean is initially at rest and is initialized with horizontally uniform temperature and salinity fields that are obtained by averaging the temperature and salinity from the World Ocean Atlas 2009 (WOA09) data over the area of 17.5°N to 22.5°N and 125°E to 140°E (fig. S4). During the integration, the model ocean is only subject to wind forcing; short-wave radiation, long-wave radiation, and air-sea turbulent heat fluxes are not included. The surface wind fields (v_s) associated with a typhoon are expressed as a modified Rankine vortex model:

$$v_s = \begin{cases} v_{\max}\dfrac{r}{r_{\max}} & \text{for } r \le r_{\max}; \\ v_{\max}\left(\dfrac{r_{\max}}{r}\right)^a & \text{for } r > r_{\max}, \end{cases}$$

where r is the distance from the typhoon center, $r_{\max}$ is the radius of maximum wind speed, $v_{\max} = 50$ m s^{-1} is the wind speed at $r_{\max}$, and a is a shape parameter. In our simulation, $r_{\max}$ is 50 km and a is 0.5 (*76*, *77*). The idealized typhoon moves from east to west at a translation speed of U, which is largely determined by environmental flows and is set to be a typical value of 4.5 m s^{-1}. This translation speed is also added to the hurricane-like wind fields, producing an asymmetry in the surface winds. To avoid large-scale upwelling and downwelling in the simulations, the addition of translation speed only applies within a circle with a radius of 600 km centered at the typhoon center. In addition, two different forms of drag coefficient as a function of wind speed are used in the calculations of wind stress (fig. S5): one is adopted from ref. (*78*) (see the red curves in their Fig. 3), and the other is very similar to the estimates by ref. (*79*), with the drag coefficient leveling

off for wind speed above 33 m s^{-1} (see their Fig. 2); these two different forms produce very similar results.

To facilitate visualizing how fast the subsurface water can be brought to the surface, we add inert tracers at various water layers peaking at 25, 75, 125, and 175 m with a concentration of 100 U. To avoid the model blow-up, the tracer concentration follows a normal distribution in the vertical with an SD of 8 m.

SUPPLEMENTARY MATERIALS

Supplementary material for this article is available at http://advances.sciencemag.org/cgi/content/full/1/4/e1500014/DC1

Materials and Methods

Fig. S1. Evolution of seasonal mean lifetime peak intensity of typhoons.

Fig. S2. Changes in proportions of TCs of different intensity.

Fig. S3. Main typhoon intensification region.

Fig. S4. Vertical profiles of temperature and salinity used to initialize the ROMS simulation.

Fig. S5. Drag coefficient as a function of surface wind speed used in ROMS simulations.

Fig. S6. Typhoon-induced changes in tracer content simulated by ROMS.

Fig. S7. Observed and simulated changes in ocean temperatures.

Fig. S8. High-frequency variations in typhoon metrics and their modulation by oceanic and climate variables.

Fig. S9. Simulated changes in various atmospheric thermodynamic variables.

Table S1. Correlation between the duration of typhoon intensification and various variables.

Table S2. Details of the ocean component of the CMIP5 models in use.

References (*80*–*90*)

REFERENCES AND NOTES

1. R. Pielke Jr., J. Gratz, C. Landsea, D. Collins, M. Saunders, R Musulin, Normalized hurricane damage in the United States: 1900–2005. *Nat. Hazards Rev.* **9**, 29–42 (2008).
2. P. Peduzzi, B. Chatenoux, H. Dao, A. De Bono, C. Herold, J. Kossin, F. Mouton, O. Nordbeck, Global trends in tropical cyclone risk. *Nat. Clim. Change* **2**, 289–294 (2012).
3. T. Lum, R. Margesson, *Typhoon Haiyan (Yolanda): U.S. and International Response to Philippines Disaster* (Congressional Research Service, Library of Congress, Washington, DC, 2014).
4. K. A. Emanuel, The maximum intensity of hurricanes. *J. Atmos. Sci.* **45**, 1143–1155 (1988).
5. G. J. Holland, The maximum potential intensity of tropical cyclones. *J. Atmos. Sci.* **54**, 2519–2541 (1997).
6. J. P. Cangialosi, J. L. Franklin, *2012 National Hurricane Center forecast verification report*; http://www.nhc.noaa.gov/verification/pdfs/Verification_2012.pdf.
7. R. T. Merrill, Environmental influences on hurricane intensification. *J. Atmos. Sci.* **45**, 1678–1687 (1988).
8. K. Emanuel, Thermodynamic control of hurricane intensity. *Nature* **401**, 665–669 (1999).
9. M. DeMaria, The effect of vertical shear on tropical cyclone intensity change. *J. Atmos. Sci.* **53**, 2076–2087 (1996).
10. L. K. Shay, G. J. Goni, P. G. Black, Effects of a warm oceanic feature on Hurricane Opal. *Mon. Weather Rev.* **128**, 1366–1383 (2000).
11. I. Ginis, Tropical cyclone–ocean interactions, in *Atmosphere–Ocean Interactions*, W. Perrie, Ed. (WIT Press, Southampton, UK, 2002), vol. 33, pp. 83–114.
12. C.-C. Wu, C.-Y. Lee, I.-I. Lin, The effect of the ocean eddy on tropical cyclone intensity. *J. Atmos. Sci.* **64**, 3562–3578 (2007).
13. W. Mei, C. Pasquero, F. Primeau, The effect of translation speed upon the intensity of tropical cyclones over the tropical ocean. *Geophys. Res. Lett.* **39**, L07801 (2012).
14. I.-I. Lin, P. Black, J. F. Price, C.-Y. Yang, S. S. Chen, C.-C. Lien, P. Harr, N.-H. Chi, C.-C. Wu, E. A. D'Asaro, An ocean coupling potential intensity index for tropical cyclones. *Geophys. Res. Lett.* **40**, 1878–1882 (2013).
15. G. A. Vecchi, G. Villarini, Next season's hurricanes. *Science* **343**, 618–619 (2014).
16. M. Zhao, I. M. Held, S.-J. Lin, G. A. Vecchi, Simulations of global hurricane climatology, interannual variability, and response to global warming using a 50-km resolution GCM. *J. Climate* **22**, 6653–6678 (2009).
17. W. Mei, S.-P. Xie, M. Zhao, Variability of tropical cyclone track density in the North Atlantic: Observations and high-resolution simulations. *J. Climate* **27**, 4797–4814 (2014).
18. W. Mei, S.-P. Xie, M. Zhao, Y. Wang, Forced and internal variability in tropical cyclone track density in the western North Pacific. *J. Climate* **28**, 143–167 (2015).
19. T. R. Knutson, J. L. McBride, J. Chan, K. Emanuel, G. Holland, C. Landsea, I. Held, J. P. Kossin, A. K. Srivastava, M. Sugi, Tropical cyclones and climate change. *Nat. Geosci.* **3**, 157–163 (2010).
20. J.-H. Chu, C. R. Sampson, A. S. Levine, E. Fukada, *The Joint Typhoon Warning Center Tropical Cyclone Best-Tracks, 1945–2000, Ref. NRL/MR/7540-02-16* (Naval Research Laboratory, Washington, DC, 2002).
21. K. A. Emanuel, Increasing destructiveness of tropical cyclones over the past 30 years. *Nature* **436**, 686–688 (2005).
22. P. J. Webster, G. J. Holland, J. A. Curry, H.-R. Chang, Changes in tropical cyclone number, duration, and intensity in a warming environment. *Science* **309**, 1844–1846 (2005).
23. C. D. Hoyos, P. A. Agudelo, P. J. Webster, J. A. Curry, Deconvolution of the factors contributing to the increase in global hurricane intensity. *Science* **312**, 94–97 (2006).
24. J. B. Elsner, J. P. Kossin, T. H. Jagger, The increasing intensity of the strongest tropical cyclones. *Nature* **455**, 92–95 (2008).
25. N.-Y. Kang, J. B. Elsner, Consensus on climate trends in the western North Pacific tropical cyclones. *J. Climate* **25**, 7564–7573 (2012).
26. G. J. Holland, C. L. Bruyère, Recent intense hurricane response to global climate change. *Clim. Dyn.* **42**, 617–627 (2014).
27. J. L. McBride, R. Zehr, Observational analysis of tropical cyclone formation. Part II: Comparison of non-developing versus developing systems. *J. Atmos. Sci.* **38**, 1132–1151 (1981).
28. J. Molinari, S. Skubis, D. Vollaro, F. Alsheimer, H. E. Willoughby, Potential vorticity analysis of tropical cyclone intensification. *J. Atmos. Sci.* **55**, 2632–2644 (1998).
29. J. C. L. Chan, Decadal variations of intense typhoon occurrence in the western North Pacific. *Proc. R. Soc. A* **464**, 249–272 (2008).
30. I. D. Lloyd, G. A. Vecchi, Observational evidence for oceanic controls on hurricane intensity. *J. Climate* **24**, 1138–1153 (2011).
31. M. Zhao, I. M. Held, TC-permitting GCM simulations of hurricane frequency response to sea surface temperature anomalies projected for the late-twenty-first century. *J. Climate* **25**, 2995–3009 (2012).
32. E. M. Vincent, K. A. Emanuel, M. Lengaigne, J. Vialard, G. Madec, Influence of upper ocean stratification interannual variability on tropical cyclones. *J. Adv. Model. Earth Syst.* **6** (2014).
33. K. Balaguru, S. Taraphdar, L. R. Leung, G. R. Foltz, J. A. Knaff, Cyclone-cyclone interactions through the ocean pathway. *Geophys. Res. Lett.* **41**, 6855–6862 (2014).
34. T. R. Knutson, J. J. Sirutis, S. T. Garner, G. A. Vecchi, I. M. Held, Simulated reduction in Atlantic hurricane frequency under twenty-first-century warming conditions. *Nat. Geosci.* **1**, 359–364 (2008).
35. G. A. Vecchi, K. L. Swanson, B. J. Soden, Whither hurricane activity? *Science* **322**, 687–689 (2008).
36. K. Emanuel, A. Sobel, Response of tropical sea surface temperature, precipitation, and tropical cyclone-related variables to changes in global and local forcing. *J. Adv. Model. Earth Syst.* **5**, 447–458 (2013).
37. H. A. Ramsay, The effects of imposed stratospheric cooling on the maximum intensity of tropical cyclones in axisymmetric radiative–convective equilibrium. *J. Climate* **26**, 9977–9985 (2013).
38. J. F. Price, Upper ocean response to a hurricane. *J. Phys. Oceanogr.* **11**, 153–175 (2009).
39. We also tried with the depth-averaged ocean temperature as suggested in ref. (57), and found that the combination of SST and 75-m temperature is a better choice because it explains more variance in TC intensification rate.
40. Theoretically, the first term should be related to potential intensity and not SST, but SST is more accurately measured.
41. W. Mei, C. Pasquero, Spatial and temporal characterization of sea surface temperature response to tropical cyclones. *J. Climate* **26**, 3745–3765 (2013).
42. M. M. Bell, M. T. Montgomery, Observed structure, evolution, and potential intensity of category 5 Hurricane Isabel (2003) from 12 to 14 September. *Mon. Weather Rev.* **136**, 2023–2046 (2008).
43. K. A. Emanuel, The dependence of hurricane intensity on climate. *Nature* **326**, 483–485 (1987).
44. K. Emanuel, Tropical cyclones. *Annu. Rev. Earth Planet. Sci.* **31**, 75–104 (2003).
45. H. A. Ramsay, A. H. Sobel, Effects of relative and absolute sea surface temperature on tropical cyclone potential intensity using a single-column model. *J. Climate* **24**, 183–193 (2011).
46. T. R. Knutson, R. E. Tuleya, Y. Kurihara, Simulated increase of hurricane intensities in a CO_2-warmed climate. *Science* **3**, 1018–1021 (1998).
47. T. R. Knutson, R. E. Tuleya, Impact of CO_2-induced warming on simulated hurricane intensity and precipitation: Sensitivity to the choice of climate model and convective parameterization. *J. Climate* **17**, 3477–3495 (2004).
48. K. E. Trenberth, C. A. Davis, J. T. Fasullo, Water and energy budgets of hurricanes: Case studies of Ivan and Katrina. *J. Geophys. Res.* **112**, D23106 (2007).
49. R. L. Korty, K. A. Emanuel, J. R. Scott, Tropical cyclone–induced upper-ocean mixing and climate: Application to equable climates. *J. Climate* **21**, 638–654 (2008).
50. J. C. L. Chan, K. S. Liu, Global warming and western North Pacific typhoon activity from an observational perspective. *J. Climate* **17**, 4590–4602 (2004).

51. S. J. Camargo, A. H. Sobel, Western North Pacific tropical cyclone intensity and ENSO. *J. Climate* **18**, 2996–3006 (2005).
52. Although it is the large-scale wind field that directly affects the location of typhoon formation, wind changes are remotely driven by SSTs in the central equatorial Pacific. We chose the SSTs in the central equatorial Pacific as predictor because they are more predictable than wind field.
53. Y. Kosaka, S.-P. Xie, Recent global-warming hiatus tied to equatorial Pacific surface cooling. *Nature* **501**, 403–407 (2013).
54. M. Mainelli, M. DeMaria, L. K. Shay, G. Goni, Application of oceanic heat content estimation to operational forecasting of recent Atlantic category 5 hurricanes. *Wea. Forecast.* **23**, 3–16 (2008).
55. I.-I. Lin, C.-C. Wu, I.-F. Pun, D.-S. Ko, Upper-ocean thermal structure and the western North Pacific category 5 typhoons. Part I: Ocean features and the category 5 typhoons' intensification. *Mon. Weather Rev.* **136**, 3288–3306 (2008).
56. G. Goni, M. DeMaria, J. Knaff, C. Sampson, I. Ginis, F. Bringas, A. Mavume, C. Lauer, I.-I. Lin, M.M. Ali, P. Sandery, S. Ramos-Buarque, K. Kang, A. Mehra, E. Chassignet, G. Halliwell, Applications of satellite-derived ocean measurements to tropical cyclone intensity forecasting. *Oceanography* **22**, 190–197 (2009).
57. J. F. Price, Metrics of hurricane-ocean interaction: Vertically-integrated or vertically-averaged ocean temperature? *Ocean Sci.* **5**, 351–368 (2009).
58. F.-F. Jin, J. Boucharel, I.-I. Lin, Eastern Pacific tropical cyclones intensified by El Niño delivery of subsurface ocean heat. *Nature* **516**, 82–85 (2014).
59. K. E. Taylor, R. J. Stouffer, G. A. Meehl, An overview of CMIP5 and the experiment design. *Bull. Amer. Meteor. Soc.* **93**, 485–498 (2012).
60. W. Shen, R. E. Tuleya, I. Ginis, A sensitivity study of the thermodynamic environment on GFDL model hurricane intensity: Implications for global warming. *J. Climate* **13**, 109–121 (2000).
61. K. A. Hill, G. M. Lackmann, The impact of future climate change on TC intensity and structure: A downscaling approach. *J. Climate* **24**, 4644–4661 (2011).
62. T.-C. Lin, S. P. Hamburg, K.-C. Lin, L.-J. Wang, C.-T. Chang, Y.-J. Hsia, M. A. Vadeboncoeur, C. M. M. McMullen, C.-P. Liu, Typhoon disturbance and forest dynamics: Lessons from a Northwest Pacific subtropical forest. *Ecosystems* **14**, 127–143 (2011).
63. C. Hongo, H. Kawamata, K. Goto, Catastrophic impact of typhoon waves on coral communities in the Ryukyu Islands under global warming. *J. Geophys. Res.* **117**, G02029 (2012).
64. K. Emanuel, Contribution of tropical cyclones to meridional heat transport by the oceans. *J. Geophys. Res.* **106**, 14771–14781 (2001).
65. R. L. Sriver, M. Huber, Observational evidence for an ocean heat pump induced by tropical cyclones. *Nature* **447**, 577–580 (2007).
66. R. E. Hart, An inverse relationship between aggregate northern hemisphere tropical cyclone activity and subsequent winter climate. *Geophys. Res. Lett.* **38**, L01705 (2011).
67. W. Mei, F. Primeau, J. C. McWilliams, C. Pasquero, Sea surface height evidence for long-term warming effects of tropical cyclones on the ocean. *Proc. Natl. Acad. Sci. U.S.A.* **110**, 15207–15210 (2013).
68. M. R. Bueti, I. Ginis, L. M. Rothstein, S. M. Griffies, Tropical cyclone–induced thermocline warming and its regional and global impacts. *J. Climate* **27**, 6978–6999 (2014).
69. E. Kalnay, M. Kanamitsu, R. Kistler, W. Collins, D. Deaven, L. Gandin, M. Iredell, S. Saha, G. White, J. Woollen, Y. Zhu, A. Leetmaa, R. Reynolds, M. Chelliah, W. Ebisuzaki, W. Higgins, J. Janowiak, K. C. Mo, C. Ropelewski, J. Wang, R. Jenne, D. Joseph, The NCEP/NCAR 40-year reanalysis project. *Bull. Amer. Meteor. Soc.* **77**, 437–471 (1996).
70. N. A. Rayner, D. E. Parker, E. B. Horton, C. K. Folland, L. V. Alexander, D. P. Rowell, E. C. Kent, A. Kaplan, Global analyses of sea surface temperature, sea ice, and night marine air temperature since the late nineteenth century. *J. Geophys. Res.* **108**, 4407 (2003).
71. S. Levitus, J. I. Antonov, T. P. Boyer, R. A. Locarnini, H. E. Garcia, A. V. Mishonov, Global ocean heat content 1955–2008 in light of recently revealed instrumentation problems. *Geophys. Res. Lett.* **36**, L07608 (2009).
72. K. Emanuel, R. Sundararajan, J. Williams, Hurricanes and global warming: Results from downscaling IPCC AR4 simulations. *Bull. Amer. Meteor. Soc.* **89**, 347–367 (2008).
73. A. F. Shchepetkin, J. C. McWilliams, The regional oceanic modeling system (ROMS): A split-explicit, free-surface, topography-following-coordinate oceanic model. *Ocean Modell.* **9**, 347–404 (2005).
74. W. Mei, C.-C. Lien, I.-I. Lin, S.-P. Xie, Tropical cyclone-induced ocean response: A comparative study of the South China Sea and tropical Northwest Pacific. *J. Climate* 10.1175/JCLI-D-14-00651.1 (2015).
75. W. G. Large, J. C. McWilliams, S. C. Doney, Oceanic vertical mixing: A review and a model with a nonlocal boundary layer parameterization. *Rev. Geophys.* **32**, 363–403 (1994).
76. K. A. Emanuel, An air-sea interaction theory for tropical cyclones. Part I: Steady-state maintenance. *J. Atmos. Sci.* **43**, 585–605 (1986).
77. K. J. Mallen, M. T. Montgomery, B. Wang, Reexamining the near-core radial structure of the tropical cyclone primary circulation: Implications for vortex resiliency. *J. Atmos. Sci.* **62**, 408–425 (2005).
78. K. J. E. Walsh, P. Sandery, G. B. Brassington, M. Entel, C. Siegenthaler-LeDrian, J. D. Kepert, R. Darbyshire, Constraints on drag and exchange coefficients at extreme wind speeds. *J. Geophys. Res.* **115**, C09007 (2010).
79. M. A. Donelan, B. K. Haus, N. Reul, W. J. Plant, M. Stiassnie, H. C. Graber, O. B. Brown, E. S. Saltzman, On the limiting aerodynamic roughness of the ocean in very strong winds. *Geophys. Res. Lett.* **31**, L18306 (2004).
80. M. R. Lowry, Developing a unified superset in quantifying ambiguities among tropical cyclone best track data for the western North Pacific, thesis, Florida State University (2008).
81. H. Koba, T. Hagiwara, S. Osano, S. Akashi, Relationship between the CI-number and central pressure and maximum wind speed in typhoons. *J. Meteor. Res.* **42**, 59–67 (1990).
82. M. C. Kruk, K. R. Knapp, D. H. Levinson, A technique for combining global tropical cyclone best track data. *J. Atmos. Oceanic Technol.* **27**, 680–692 (2010).
83. V. F. Dvorak, *Tropical Cyclone Intensity Analysis Using Satellite Data (Technical Report NESDIS 11)* (National Oceanic and Atmospheric Administration, Washington, DC, 1984).
84. L. Wu, H. Zhao, Dynamically derived tropical cyclone intensity changes over the western North Pacific. *J. Climate* **25**, 89–98 (2012).
85. J. P. Kossin, T. L. Olander, K. R. Knapp, Trend analysis with a new global record of tropical cyclone intensity. *J. Climate* **26**, 9960–9976 (2013).
86. K. R. Knapp, J. A. Knaff, C. R. Sampson, G. M. Riggio, A. D. Schnapp, A pressure-based analysis of the historical western North Pacific tropical cyclone intensity record. *Mon. Wea. Rev.* **141**, 2611–2631 (2013).
87. C. P. Guard, L. E. Carr, F. H. Wells, R. A. Jeffries, N. D. Gural, D. K. Edson, Joint Typhoon Warning Center and the challenges of multibasin tropical cyclone forecasting. *Wea. Forecast.* **7**, 328–352 (1992).
88. J. D. Martin, W. M. Gray, Tropical cyclone observation and forecasting with and without aircraft reconnaissance. *Wea. Forecast.* **8**, 519–532 (1993).
89. J. A. Knaff, D. P. Brown, J. Courtney, G. M. Gallina, J. L. Beven II, An evaluation of Dvorak technique–based tropical cyclone intensity estimates. *Wea. Forecast.* **25**, 1362–1379 (2010).
90. W. M. Gray, *Tropical Cyclone Genesis* (Colorado State University, Fort Collins, CO, 1975).

Acknowledgments: We thank K. Emanuel for sharing the compiled TC best track data. We thank C. Garrett (editor), K. Emanuel (reviewer), and the anonymous reviewers for their valuable comments that helped improve the manuscript. **Funding:** This work was funded by NASA Headquarters under the NASA Earth and Space Science Fellowship Program grant NNX10AP30H, NSF grant AGS-1305719, and National Oceanic and Atmospheric Administration grant NA13OAR4310092. C.P. acknowledges support from CINECA grant LISA MAREVENT and from the Italian Ministry MIUR under the National Research Program, project RITMARE. **Author contributions:** W.M. conceived the project and designed and performed the analyses. All authors contributed to the interpretation of the results and the writing of the manuscript. **Competing interests:** The authors declare that they have no competing interests.

Submitted 7 January 2015
Accepted 16 April 2015
Published 29 May 2015
10.1126/sciadv.1500014

Citation: W. Mei, S.-P. Xie, F. Primeau, J. C. McWilliams, C. Pasquero, Northwestern Pacific typhoon intensity controlled by changes in ocean temperatures. *Sci. Adv.* **1**, e1500014 (2015).